Opto-Electronic Science

CN 51–1800/O4 ISSN 2097–0382 (Print) ISSN 2097–4000 (Online)

High fiber-to-fiber net gain in erbium-doped thin film lithium niobate waveguide amplifier as an external gain chip

Jinli Han, Mengqi Li, Rongbo Wu, Jianping Yu, Lang Gao, Zhiwei Fang, Min Wang, Youting Liang, Haisu Zhang and Ya Cheng

Citation: Han JL, Li MQ, Wu RB, et al. High fiber-to-fiber net gain in erbium-doped thin film lithium niobate waveguide amplifier as an external gain chip. *Opto-Electron Sci* **4**, 250004 (2025).

https://doi.org/10.29026/oes.2025.250004

Received: 18 February 2025; Accepted: 7 April 2025; Published online: 13 June 2025

Related articles

Spatio-temporal isolator in lithium niobate on insulator

Haijin Huang, Armandas Balčytis, Aditya Dubey, Andreas Boes, Thach G. Nguyen, Guanghui Ren, Mengxi Tan, Arnan Mitchell

Opto-Electronic Science 2023 **2**, 220022 doi: 10.29026/oes.2023.220022

Exceptional-point-enhanced sensing in an all-fiber bending sensor

Zheng Li, Jingxu Chen, Lingzhi Li, Jiejun Zhang, Jianping Yao

Opto-Electronic Advances 2023 **6**, 230019 doi: 10.29026/oea.2023.230019

Ferroelectric domain engineering of Lithium niobate

Jackson J. Chakkoria, Aditya Dubey, Arnan Mitchell, Andreas Boes

Opto-Electronic Advances 2025 **8**, 240139 doi: 10.29026/oea.2025.240139

A tunable nanosecond pulse mode-locking fiber laser

Liu Yuxing, Jiang Panqiu, Wang Pinghe

Opto-Electronic Engineering 2021 **48**, 210195 doi: 10.12086/oee.2021.210195

Opto-Electronic Science

Article

2025, Vol. 4, No.

DOI: 10.29026/oes.2025.250004 CSTR: 32246.14.oes.2025.250004

High fiber-to-fiber net gain in erbium-doped thin film lithium niobate waveguide amplifier as an external gain chip

Jinli Han[1,2], Mengqi Li[2], Rongbo Wu[2], Jianping Yu[2], Lang Gao[3], Zhiwei Fang[2], Min Wang[2], Youting Liang[2]*, Haisu Zhang[2]* and Ya Cheng[1,2,3,4,5,6,7]*

Miniaturized erbium-doped waveguide amplifiers attracted great interests in recent decades due to their high gain-efficiency and function-scalability in the telecom C-band. In this work, an erbium-doped thin film lithium niobate waveguide amplifier achieving >10 dB off-chip (fiber-to-fiber) net gain and >20 mW fiber-output amplified power is demonstrated, thanks to the low-propagation-loss waveguides and robust waveguide edge-couplers prepared by the photolithography assisted chemomechanical etching technique. Systematic investigation on the fabricated waveguide amplifiers reveals remarkable optical gain around the peak wavelength of 1532 nm as well as the low fiber-coupling loss of −1.2 dB/facet. A fiber Bragg-grating based waveguide laser is further demonstrated using the fabricated waveguide amplifier as the external gain chip, which generates >2 mW off-chip power continuous-wave lasing around the gain peak at 1532 nm. The unambiguous demonstration of fiber-to-fiber net gain of the erbium-doped thinfilm lithium niobate (TFLN) waveguide amplifier as well as its external gain chip application will benefit diverse fields demanding scalable gain elements with high-speed tunability.

Keywords: integrated photonics; thin-film lithium niobate; erbium doped waveguide amplifier

Han JL, Li MQ, Wu RB et al. High fiber-to-fiber net gain in erbium-doped thin film lithium niobate waveguide amplifier as an external gain chip. *Opto-Electron Sci* **4**, 250004 (2025).

Introduction

Erbium-doped waveguide amplifiers and lasers have been intensively investigated in recent decades, motivated by the prevalent success of erbium doped fibers in a plethora of excellent applications such as power amplifiers and ultrafast lasers[1−3]. The distinct advantage of erbium-doped waveguides stems from their high-mode-confinement compared to the erbium-doped fiber, entailing low power consumption and compact footprint[4−10]. The highly confined waveguide modes also

[1]State Key Laboratory of Precision Spectroscopy, East China Normal University, Shanghai 200062, China; [2]The Extreme Optoelectromechanics Laboratory (XXL), School of Physics and Electronic Sciences, East China Normal University, Shanghai 200241, China; [3]State Key Laboratory of High Field Laser Physics and CAS Center for Excellence in Ultra-Intense Laser Science, Shanghai Institute of Optics and Fine Mechanics (SIOM), Chinese Academy of Sciences (CAS), Shanghai 201800, China; [4]Hefei National Laboratory, Hefei 230088, China; [5]Shanghai Research Center for Quantum Sciences, Shanghai 201315, China; [6]Collaborative Innovation Center of Extreme Optics, Shanxi University, Taiyuan 030006, China; [7]Collaborative Innovation Center of Light Manipulations and Applications, Shandong Normal University, Jinan 250358, China.
*Correspondence: YT Liang, E-mail: ytliang@phy.ecnu.edu.cn; HS Zhang, E-mail: hszhang@phy.ecnu.edu.cn;
Y Cheng, E-mail: ya.cheng@siom.ac.cn

Received: 18 February 2025; Accepted: 7 April 2025 ; Published online: 13 June 2025

exert strong limitations on the optical coupling of erbium-doped waveguides with optical fibers and free-space optics in practical applications. Furthermore, erbium-doped waveguide amplifiers and lasers are usually characterized using fiber-coupled off-chip measurements, with the on-chip gain and power extrapolated by prescribed coupling losses[11–19]. The measured off-chip gain and power are quite limited and negative fiber-to-fiber gains often exist in planar waveguide amplifiers of large coupling losses. Even worse situation emerges when the coupling status fluctuates during experiments, impeding reliable retrievals of on-chip gain and power from separate off-chip measurements.

In this work, by employing the erbium-doped thin film lithium niobate (TFLN) waveguides fabricated by the photolithography assisted chemomechanical etching (PLACE) technique, high-gain erbium-doped waveguide amplifiers (EDWA) are built with robust edge-couplers prepared by the same technique[20,21]. Fiber-to-fiber net gains are unambiguously established in the TFLN based EDWAs, thanks to the low-propagation-loss waveguides and the low-coupling-loss edge couplers both fabricated by the PLACE technique. Experimental characterization reveals >10 dB off-chip small-signal gains at the gain peak wavelength around 1532 nm, and the maximum fiber-output amplified signal power is 20.26 mW (13.07 dBm) at the fiber-input power of 9.77 mW (9.89 dBm). Further measurements on the saturated absorption losses and signal enhancement factors of the TFLN-EDWA pinpoint the inadequate gain retrieval method adopted by most TFLN-EDWA researches, which can overestimate the on-chip gain to a large extent. Besides, gain saturation measurements of the amplified spontaneous emissions unveil the distinct contributions from both the homogeneous and inhomogeneous spectral broadening of erbium ions in TFLN. To utilize the high-gain EDWA as an external gain chip, a fiber Bragg-grating (FBG) based laser cavity is built which can generate >2 mW off-chip power continuous-wave lasing around 1532 nm. To the best of our knowledge, this is the first FBG-based EDWA laser on the TFLN platform with the largest off-chip laser power. The demonstrated high-gain EDWAs hold great promise in various applications demanding scalable gain elements with high-speed tunability.

Results

Design and fabrication of the TFLN-EDWA

The TFLN-EDWA is built on the erbium-doped *Z*-cut lithium niobate on insulator (LNOI) wafer prepared by the ion-slicing process (NanoLN, Jinan Jingzheng) from the congruent erbium-doped lithium niobate bulk crystal. The erbium-doping concentration is 0.5 mol%. The top LN layer thickness is 500 nm, and the buried oxide layer and the bottom silicon substrate are 4.7 μm thick and 500 μm thick, respectively. The TFLN waveguide is fabricated by the PLACE technique consisting of femtosecond laser patterning and chemomechanical polishing[20,21]. Straight waveguide structures are adopted in this work to facilitate the modal field expansion by adiabatic waveguide tapers as shown in Fig. 1(a). The large-mode-area TFLN amplifier was previously found to support high-power amplification[22]. Edge couplers using the spot-size-convertor (SSC) are further built on both ends of the TFLN waveguides[23,24]. The SSC components are formed by first producing a vertical taper at the end of the TFLN waveguide and then covering the tapered TFLN waveguide with the 3 μm thick SiON thin film, which are further dry etched into strip waveguides facilitating fiber coupling. Such kind of structure has been verified in previous works on the passive TFLN platform which enables the adiabatic mode conversion from the underneath TFLN waveguide to the over-cladding SiON-waveguide. Fabrication details can be found in the previous work[23]. The simulated modal evolution around the SSC region is shown in Fig. 1(b), where the top panel shows the vertical mode evolution from the TFLN waveguide to the SiON waveguide and the middle panels (i–v) depict the cross-section mode profiles at different propagation positions.

The output mode profile from the SSC-port is measured by an infrared camera and shown in Fig. 1(c), where a symmetric mode shape is obtained. For comparison, the output mode profile of the ultrahigh-NA fiber (UHNA7) is also measured and shown in Fig. 1(d). The UHNA7 fiber has the *NA*=0.41 and a mode field diameter (MFD) of 3.2 μm at 1550 nm. The modal overlap between the mode profiles of the SSC-port and the UHNA7 fiber is estimated to be >90%. As a result, the SSC-ports integrated on the TFLN-waveguides can realized high-efficiency coupling with UHNA7 fibers. A fluorescence microscope image around the SSC region is shown in the bottom panel of Fig. 1(b), where the input pump light is coupled into the SSC-port from the right side and then gradually evolves into the erbium-doped TFLN-waveguide featuring bright up-conversion fluorescence emanated from excited erbium ions.

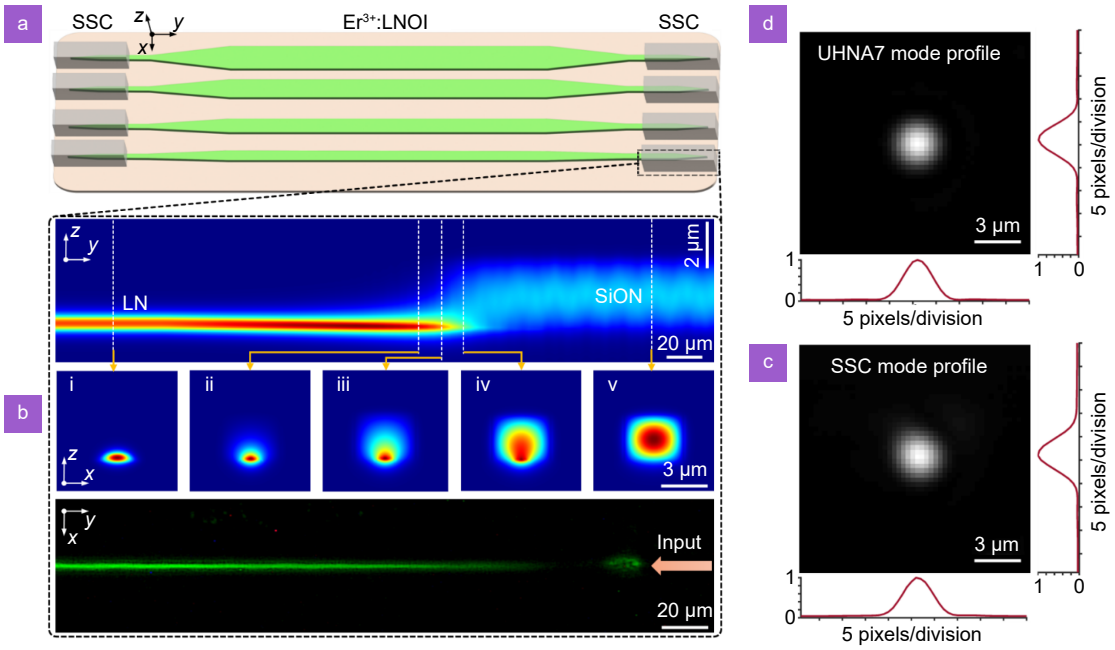

Fig. 1 | Design and modal evolution of the SSC-integrated EDWA chip. (**a**) the schematic of the SSC-integrated EDWA chip. (**b**) The simulated modal evolution in the SSC region with the insets (i–v) showing the cross-section modal distribution at different propagation positions (dashed lines). The bottom inset shows the fluorescence microscope image of the SSC region. (**c**) The measured SSC-output mode profile. (**d**) The measured UHNA7 output mode profile.

Experimental characterization of the EDWA chip

The experimental characterization setup for the SSC-integrated TFLN-EDWA chip is shown in Fig. 2(a). Two fiber-coupled high-power laser diodes at the wavelength of 1480 nm are used as the pumps, and a C-band tunable external cavity continuous-wave diode laser (toptica) is used as the signal. The signal laser and one pump laser are combined by the fiber-based wavelength division multiplexer (WDM) and then connected to the standard single-mode fiber (SMF) which is fusion-spliced with the UHNA7 fiber. The splicing loss between the SMF fiber and the UHNA7 fiber is measured to be −1.3 dB. The UHNA7 fiber is positioned in close contact with the SSC-port of the EDWA chip by a high-resolution three-dimensional motorized stage, and index-matching gels are dripped to the coupling interface for Fresnel-reflection suppression. The other pump laser is similarly guided through the fiber-WDM and the SMF-spliced UHNA7 fiber, and then injected into the EDWA chip. The output signal is measured after the second fiber-WDM by the optical spectrum analyzer (OSA) as well as high-resolution power meters. Fiber-based polarization controllers (PC) are inserted in both pump laser and signal laser paths for excitation of the transverse-electric (TE) modes in the TFLN waveguides of the length of 5.5 cm.

The relevant energy-level diagram of erbium ions is shown in Fig. 2(b). The transition between the first excited-level $^4I_{13/2}$ and the ground-level $^4I_{15/2}$ peaked at 1532 nm is responsible for the optical gain in the telecom C-band. Cooperative up-conversions between excited-levels $^4I_{13/2}$ and $^4I_{11/2}$ populate higher excited-levels responsible for the green fluorescence emissions. Stark-splitting induced by the crystalline field divides the $^4I_{13/2}$ and $^4I_{15/2}$ levels into 7 and 8 sublevels named as Y_1–Y_7 and Z_1–Z_8 in the literature[25]. All the transitions between the thermalized Stark-level manifolds of both levels ($^4I_{13/2}$ and $^4I_{15/2}$) form the broad absorption and emission bands of erbium ions, which are further perturbed by the linewidth broadening mechanisms in the host materials. For Er^{3+}:$LiNbO_3$, the inhomogeneous broadening linewidth is 180 GHz and the individual Stark-level transitions are identifiable even at room temperature[26]. The measured photoluminescence spectrum from Er-TFLN waveguide excited by the low-power signal laser at 1532 nm is shown in Fig. 2(c), where a few Stark-level transitions are clearly observed and labeled. The in-band pumping by the 1480 nm laser corresponds to the transitions from the lowest Stark-level Z_1 of ground-state $^4I_{15/2}$ to the higher Stark-levels (Y_6–Y_7) of excited-state $^4I_{13/2}$.

The fiber-to-fiber net gain of the EDWA chip is first measured with increasing signal input powers by directly

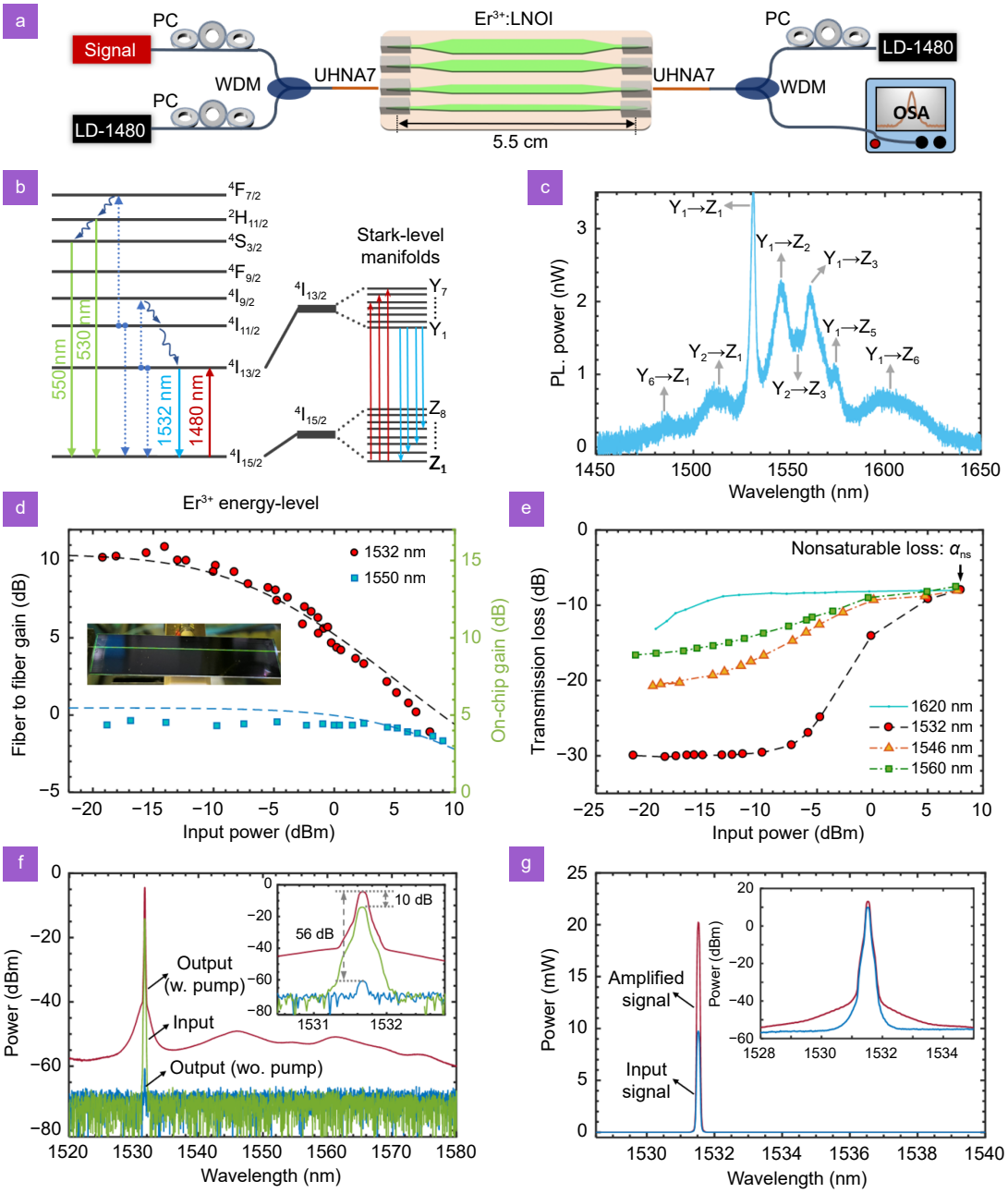

Fig. 2 | Gain characterization of the EDWA chip. (**a**) The experimental schematic. (**b**) The Er^{3+} energy-level diagram. (**c**) The photoluminescence spectrum from the TFLN-waveguide. (**d**) The fiber-to-fiber net gain curves measured at two different signal wavelengths. (**e**) The fiber-to-fiber transmission loss curves measured at four different signal wavelengths. (**f**) The spectra of the input signal and the output signal with/without pump measured at −14 dBm input power. (**g**) The input and output signal spectra measured at 10 dBm input power. The insets in (**f**) and (**g**) show the enlarged spectra around the signal wavelength.

comparing the input signal power and the collected output signal power both in the SMF fibers at the input and output ends. The total pump power measured at the input SMF fibers from both directions is fixed at 200 mW. The measured optical gains at the signal wavelengths of 1532 nm and 1550 nm are shown in the Fig. 2(d) with the digital camera picture of the pumped EDWA chip shown in the inset. The maximum fiber-to-fiber gain is around 10.5 dB at the wavelength of 1532 nm, and the gain saturates with increasing input powers due to the reduction of population inversion. Meanwhile, the fiber-to-fiber gains at the wavelength of 1550 nm are limited around 0 dB with less variations at increasing input powers. The measured fiber-to-fiber gains $G(\lambda)$ can be

expressed as below:

$$G(\lambda) = 10\log_{10}\frac{P_{\text{out}}(\lambda)}{P_{\text{in}}(\lambda)} = 2\alpha_{\text{sl}}(\lambda) + 2\alpha_{\text{c}}(\lambda) + G_0(\lambda) \ , \tag{1}$$

where P_{in} and P_{out} are the measured signal powers at the input and output SMF fibers, α_{sl} is the splicing loss between the SMF fiber and the UHNA7 fiber, α_{c} is the coupling loss between the UHNA7 fiber and the EDWA-chip, and G_0 is the on-chip net gain of the TFLN-waveguide. Using passive TFLN waveguides (without Er-doping) with similar SSC-ports on both ends, the fiber-to-fiber insertion losses are measured to be −5 dB at 1550 nm, from which the coupling loss between the UHNA7 fiber and the SSC-port is deduced to be $\alpha_{\text{c}} = -1.2$ dB, considering the measured splicing loss of $\alpha_{\text{sl}} = -1.3$ dB (propagation losses in short TFLN waveguides can be ignored due to the smooth sidewalls prepared by the PLACE technique). By supposing the identical coupling losses between the UHNA7 fiber and the SSC-integrated EDWA chip, the on-chip net gains are extrapolated from the measured off-chip gains and shown in the right axis of Fig. 2(d).

The optical on-chip net gains (~15 dB/5.5 cm at 1532 nm) deduced by the off-chip fiber-to-fiber gain measurements are smaller compared to previously reported values from similar TFLN-EDWAs due to a few reasons as below. The employed pump laser at 1480 nm will induce incomplete population inversion due to the stimulated emissions from the excited-level by the pump laser, while the previously used 980 nm pump laser can generate nearly full inversion due to the negligible stimulated emissions at this pump wavelength. However, the relatively long lifetime of the upper excited-level $^4I_{11/2}$ is adverse for high-power amplifications due to the bottlenecking effects of $^4I_{11/2}$ first proposed in Ti-diffused lithium niobate EDWAs, and a large number of guided modes at 980 nm are also undesired for homogeneous gain distribution within the waveguide which are otherwise absorbing due to the unexcited erbium ions[27–30]. Thus, the optical gains of TFLN-EDWAs pumped at 980 nm are only prominent at short waveguide lengths and low signal powers[11–17]. In contrast, the TFLN-EDWAs pumped at 1480 nm support longer gain lengths and high-power amplifications due to the better mode-overlaps between the signal and the pump as well as the high quantum efficiency by in-band pumping.

On the other hand, the popularly employed signal-enhancement methods for characterizing the TFLN-EDWAs by comparing the output signals with the pump light turned on and off are obscured by the waveguide loss subtractions and the coupling stabilities during the on-off measurements. The signal-enhancement (SE) factor is defined as:

$$\text{SE}(\lambda) = 10\log_{10}\frac{P_{\text{on}}(\lambda)}{P_{\text{off}}(\lambda)} = G_0(\lambda) - \alpha_{\text{p}}(\lambda)\cdot L - \alpha_{\text{ab}}(\lambda)\cdot L \ , \tag{2}$$

where P_{on} and P_{off} are the measured signal output powers with the pump turned on and off, α_{p} is the passive propagation loss (scattering loss) in the waveguide and α_{ab} is the erbium absorption loss in the unpumped waveguide, L is the waveguide length, G_0 is the on-chip net gain. From the above expression one can clearly notice that a large signal enhancement factor is not necessarily corresponding to a large on-chip gain especially for the peak gain wavelength around 1532 nm where the absorption cross section is also maximized[19]. Two prerequisites exist for the reliable gain retrieval by the signal enhancement method: 1) The waveguide loss including both the passive propagation loss and the erbium absorption loss has to be accurately measured; 2) The coupling status between the input/output fibers and the waveguide amplifier has to be fixed when the pump light is turned on and off. The first requirement makes sure that the real on-chip gains can be deduced from the measured SE-factors and the second requirement guarantees the accurate definition of the SE-factor from output signal powers measured at the same coupling conditions and thus the same on-chip input signal powers. As for TFLN waveguides of large coupling losses both requirements are difficult to fulfill as described below.

To this end, the fiber-to-fiber transmission losses of the SSC-integrated EDWA chips without pump are further measured at four different signal wavelengths corresponding to the Stark-level transitions from Y_1 of the excited-level $^4I_{13/2}$ to Z_1–Z_6 of the ground-level $^4I_{15/2}$. The results are shown in Fig. 2(e). It can be clearly seen that the transmission losses are greatly reduced at higher input powers due to the ground-state depletion for all the investigated wavelengths except 1620 nm, where the transmission losses are almost constant (the loss variation for input signal power <−15 dBm is ascribed to the artefact of the input laser source near its emission band-edge). Since the thermal population of higher-Stark levels Z_6–Z_8 are very limited at room temperature the

absorption loss at 1620 nm will be negligible which gives the power-independent losses observed for this wavelength. Furthermore, at high signal powers all the transmission loss curves converge to the same value of −7.5 dB labelled as the unsaturable loss α_{ns} in Fig. 2(e). After subtracting the power-independent fiber-slicing loss $2\alpha_{sl}$ and the facet coupling loss $2\alpha_c$ from the measured unsaturable transmission loss α_{ns}, a remaining loss of −2.5 dB is obtained and its physical origin needs further investigations.

The observed wavelength- and power-dependent absorption losses from the TFLN-EDWAs exert stringent limitations on the on-chip gain retrieval by the signal enhancement method. Basically, the precise absorption loss measurements in TFLN-EDWAs of high facet-coupling losses are difficult due to the variations of coupling status at different signal wavelengths and powers induced by thermal/photorefractive effects as well as mechanical misalignment. Such obtained absorption losses will be easily underestimated by coupling-loss fluctuations (the variations of on-chip signal powers). Inadequate loss subtractions from the signal enhancement factors will then overestimate the on-chip gain deviating from the practical value. In this regard, the high-efficiency edge couplers employed in this work also enable the stable coupling of the EDWA chips with optical fibers, rendering high-precision gain and loss measurements available.

The input signal spectrum and the output signal spectra with/without the pump are further shown in Fig. 2(f). The input signal power measured before the SMF-UHNA7 fiber is −14 dBm. It can be clearly seen that the signal enhancement factor is as high as 56 dB in this case, though the measured fiber-to-fiber net gain is only 10 dB. The deduced on-chip net gain from the measured off-chip gain is around 15 dB, implying that a total waveguide loss of −41 dB, which corresponds to a waveguide unit loss of −7.5 dB/cm, has to be removed from the signal enhancement factor in order to get the real on-chip gain value. Such high loss value is mainly dominated by the erbium absorption which is highly power-sensitive and thus difficult to measure by the resonator-quality-factor method used in previous works[11–17].

Besides, a broad spectrum of amplified spontaneous emissions emerges in the amplified signal shown in Fig. 2(f), from which the amplifier noise figure (NF) is extracted as *NF*=6.8 dB by the optical source subtraction method[5]. At the maximum input signal power around 10 mW, the amplified signal power from the EDWA chip measured in the output SMF fiber is above 20 mW, and the total input pump powers are also increased to 300 mW for high-power signal amplification. The corresponding optical spectra are shown in Fig. 2(g), from which the noise figure is calculated to be *NF*=13.4 dB. The greatly increased noise figure arises from the reduced gain (*G*=3.2 dB) at the high input signal power.

The amplified spontaneous emissions (ASE) of the EDWA chip are also characterized at different pump powers, in order to investigate the underlying population inversion distribution along the full waveguide length. It is well known that the spectral shape of ASE depends on the average population inversion as well as the propagation direction in the amplifier[31]. For ASE measurements only one pump laser is used to excite the TFLN-waveguide and the generated ASE propagating in the same and inverse directions to the input pump is measured and named as forward-ASE and backward-ASE, respectively. The results are shown in Fig. 3(a) and 3(b). It can be easily noticed that the spectral shapes of the forward-ASE and the backward-ASE are identical, and the ASE-peak at 1532 nm increases quickly with the increasing pump powers in both cases. Besides, the backward-ASE power is slightly higher (25%) than the forward-ASE power, which reflects the reduced pump power and thus lower population inversion in the trailing part of EDWA. The power-evolution of the ASE spectral components at 1532 nm, 1546 nm and 1562 nm are plotted in the insets of Fig. 3(a) and 3(b). Gain saturation at 1532 nm prevails over the other spectral components which implies high population inversion fractions in the EDWA chip.

The normalized ASE spectra at low (unsaturated) and high (saturated) pump powers are shown in Fig. 3(c). Remarkable gain narrowing at the ASE-peak wavelength of 1532 nm can be clearly seen. The retrieved linewidths (full width at half maximum) of the 1532 nm peak are further plotted in Fig. 3(d), and the corresponding linewidths in frequencies are labelled in the right axis. The minimum linewidth of 1.4 nm (180 GHz) is in consistent with the inhomogeneous broadening of erbium ions in lithium niobate crystals due to local crystalline site variations. The 1532 nm ASE-linewidth before gain saturation consists of both the homogeneous broadening and the inhomogeneous broadening, with the homogeneous broadening being narrowed at increasing gains[32]. Theoretical modeling of the EDWA gain and ASE evolution is elaborated in the supplemental information.

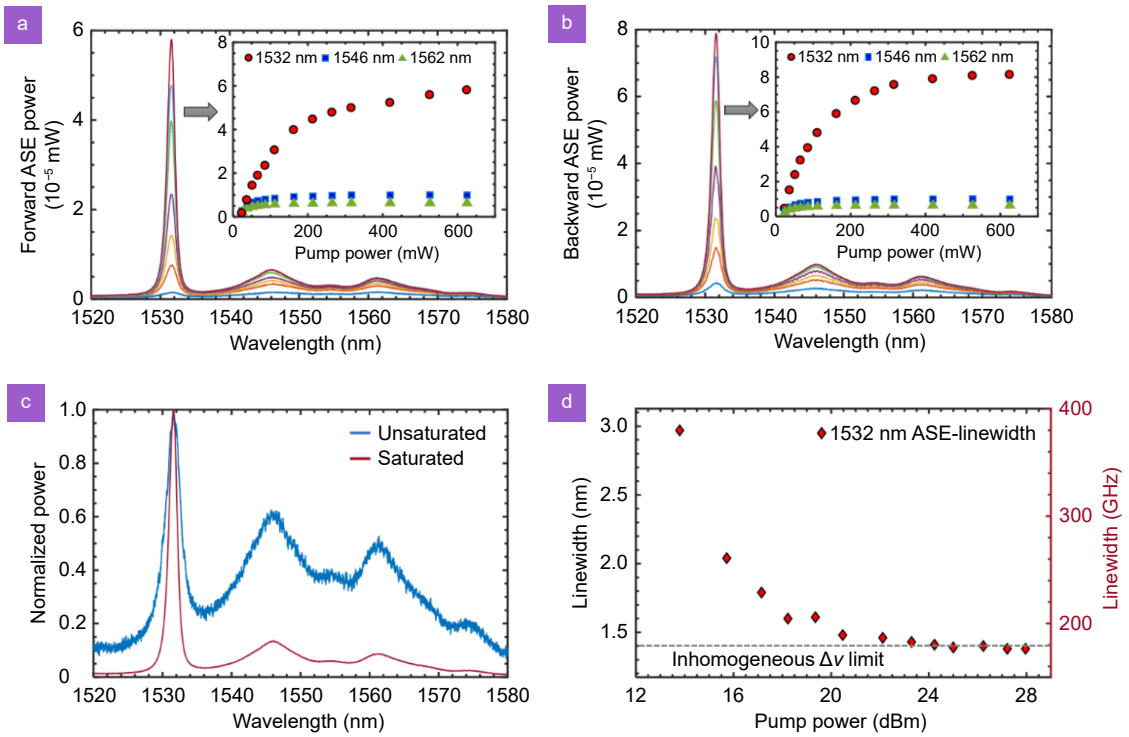

Fig. 3 | Gain saturation of the ASE from the EDWA chip. (**a**) Forward ASE spectra evolution with pump powers. (**b**) Backward ASE spectra evolution with pump powers. (**c**) The normalized ASE spectra at low (unsaturated) and high (saturated) pump powers. (**d**) The spectral linewidths of the ASE-peak at 1532 nm vs pump powers. The insets in (**a**) and (**b**) show the ASE power saturation at three different wavelengths.

External laser generation using the EDWA chip

To take advantage of the high fiber-to-fiber gain of the SSC-integrated EDWA chip, a fiber Bragg-grating (FBG) based laser cavity is built using the EDWA chip as the external gain element. The experimental schematic is shown in Fig. 4(a). Two FBGs at the center wavelength of 1532 nm are inserted between the UHNA7 fiber and the input SMF fiber to form the Fabry-Perot (FP) type laser resonator. The left FBG with the reflection rate of 99% serves as the high-reflection mirror and the right FBG with variable reflection rates is used as the laser output mirror in linear FP-cavities. Bidirectional pumping of the EDWA chip is employed. The output laser signals are separated from the residue pump and then measured by the optical spectrum analyzer (OSA). The key factor of this laser cavity application is the low coupling loss between the EDWA chip and the connecting fiber which can guarantee large off-chip gains for external laser oscillations.

The measured reflection spectra of two FBGs with 30% and 99% reflections are shown in Fig. 4(b), where the 3 dB reflection bandwidths are 1.3 nm and 0.14 nm at the center wavelength of 1532 nm, respectively. By increasing the coupled pump powers above 40 mW, a sharp lasing peak around 1532 nm emerges in the output spectra and the corresponding spectral evolution is shown in the inset of Fig. 4(c). The generated laser powers increase linearly with coupled pump powers, from which the laser slope efficiency is fitted to be 1.1%. The maximum laser power measured in the output fiber is 2.1 mW, with the corresponding laser spectrum shown in Fig. 4(d). The enlarged spectrum in the inset shows the laser linewidth of 0.1 nm, which is roughly determined by the reflection bandwidth of the output FBG coupler. It is noted that the effective laser cavity length is larger than 1 m (including the FBG fiber length and the UHNA7 fiber length), giving the longitudinal mode spacing of the order of 100 MHz (1 pm). Thus, the measured laser linewidth by OSA should be the average linewidth of multiple longitudinal modes. Different FBG output couplers are also tested and the output laser spectra at the maximum power in each case are shown in Fig. 4(e). Due to fabrication fluctuations of FBGs with different reflection rates, the generated laser wavelengths are shifted around 1532 nm and the highest laser output power is obtained with the FBG output coupler of 30% reflection. The output power of the FBG based EDWA laser can be further improved by increasing the waveguide length for

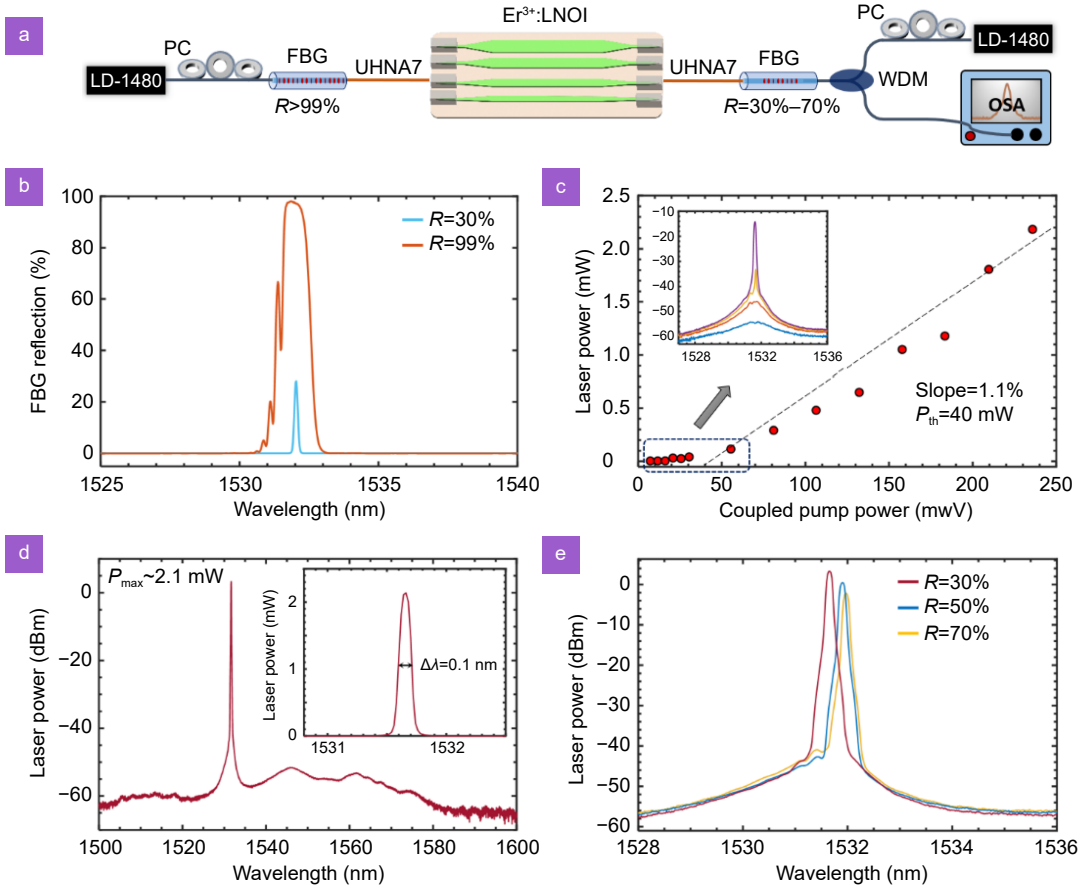

Fig. 4 | External laser generation using the EDWA chip. (**a**) The experimental schematic. (**b**) The reflection spectra of the FBGs with two different rates. (**c**) The generated laser powers vs coupled pump powers, with the laser spectra evolution around the pump threshold shown in the inset. (**d**) The laser spectrum at the maximum output power of 2.1 mW with the enlarged laser spectral profile shown in the inset. (**e**) The generated laser spectra with the FBG output couplers of different reflection rates.

higher gains and reducing the cavity losses including the fiber coupling loss, the SMF-UHNA7 splicing loss, as well as the intrinsic FBG loss. On-chip integration of laser cavity using waveguide Bragg gratings and Sagnac-loop reflectors are also feasible for compact EDWA laser sources. The external gain chip application demonstrates the potential usage of the fabricated EDWA chip as embedded gain elements in various chip-scale applications.

Discussion

The EDWAs on the TFLN platform have been broadly investigated in recent few years due to the advent of Er-doped TFLN wafers and the desire for high-density integration of multifunctional photonic chips. Previous works focused on either the attainable internal (on-chip) net gains at small-signal regimes or the on-chip integration with various functions, paying less attention on the high-efficiency fiber-waveguide coupling. The waveguide end facet coupling in EDWAs is of high importance since it will not only limit the input and output powers but also affect the gain dynamics, i.e., the signal amplification can be perturbed by amplifier parasitic lasing induced by back-reflections at the index-mismatched facets[33]. In this regard, the realized index-matched edge couplers in this work provide both high-efficiency fiber coupling and large-reduction of back-reflection: no parasitic lasing is observed even at the maximum pump powers. Meanwhile, the demonstrated EDWA chip provides the highest off-chip gain among the TFLN-EDWAs demonstrated so far (detailed comparisons can be found in the supplemental materials). From practical view of applications, the EDWA chip has to be further improved with higher off-chip gain and wider bandwidth compared to the commercial EDFAs which can routinely provide 20–30 dB fiber-to-fiber net gains covering the full telecom C-band and >20 dBm maximum output powers.

To conclude, a high-gain TFLN-EDWA chip with integrated edge-couplers achieving fiber-to-fiber (off-chip) net gains in the telecommunication C-band is demonstrated in this work. Fiber coupling losses of the EDWA chip as low as −1.2 dB/facet are realized by the spot-size-convertor between the TFLN-waveguide and the over-cladding SiON-waveguide. Through systematic characterizations of the fiber-to-fiber gains and losses of the EDWA chip, reliable on-chip net gains above 15 dB are revealed at the gain peak wavelength of 1532 nm. Experimental measurements on the spectral profiles of the ASE signals from the EDWA chip confirm the high population inversion distributed within the full waveguide length, and the gain saturation of ASE discriminates the linewidth contribution from both the homogeneous broadening and inhomogeneous broadening of erbium ions in TFLNs. To utilize the high-gain EDWA as an external gain chip, a fiber Bragg-grating based laser cavity is built which can generate >2 mW off-chip power continuous-wave lasing around 1532 nm. The demonstrated high fiber-to-fiber net gain EDWAs hold great promise in various applications demanding scalable gain elements with high-speed tunability.

References

1. Poole SB, Payne DN, Mears RJ et al. Fabrication and characterization of low-loss optical fibers containing rare-earth ions. *J Lightwave Technol* **4**, 870–876 (1986).
2. Mears RJ, Reekie L, Jauncey IM et al. Low-noise erbium-doped fibre amplifier operating at 1.54μm. *Electron Lett* **23**, 1026–1028 (1987).
3. Jauregui C, Limpert J, Tünnermann A. High-power fibre lasers. *Nat Photonics* **7**, 861–867 (2013).
4. Bradley JDB, Pollnau M. Erbium-doped integrated waveguide amplifiers and lasers. *Laser Photonics Rev* **5**, 368–403 (2011).
5. Liu Y, Qiu ZR, Ji XR et al. A photonic integrated circuit-based erbium-doped amplifier. *Science* **376**, 1309–1313 (2022).
6. Vázquez-Córdova SA, Dijkstra M, Bernhardi EH et al. Erbium-doped spiral amplifiers with 20 dB of net gain on silicon. *Opt Express* **22**, 25993–26004 (2014).
7. Brüske D, Suntsov S, Rüter CE et al. Efficient ridge waveguide amplifiers and lasers in Er-doped lithium niobate by optical grade dicing and three-side Er and Ti in-diffusion. *Opt Express* **25**, 29374–29379 (2017).
8. Mu JF, Dijkstra M, Korterik J et al. High-gain waveguide amplifiers in Si_3N_4 technology via double-layer monolithic integration. *Photonics Res* **8**, 1634–1641 (2020).
9. Bonneville DB, Osornio-Martinez CE, Dijkstra M et al. High on-chip gain spiral Al_2O_3: Er^{3+} waveguide amplifiers. *Opt Express* **32**, 15527–15536 (2024).
10. Jia YC, Wu JW, Sun XL et al. Integrated photonics based on rare-earth ion-doped thin-film lithium niobate. *Laser Photonics Rev* **16**, 2200059 (2022).
11. Chen ZX, Xu Q, Zhang K et al. Efficient erbium-doped thin-film lithium niobate waveguide amplifiers. *Opt Lett* **46**, 1161–1164 (2021).
12. Luo Q, Yang C, Hao ZZ et al. On-chip erbium-doped lithium niobate waveguide amplifiers. *Chin Opt Lett* **19**, 060008 (2021).
13. Yan XS, Liu YA, Wu JW et al. Integrated spiral waveguide amplifiers on erbium-doped thin-film lithium niobate. arXiv: 2105.00214, 2021. https://doi.org/10.48550/arXiv.2105.00214.
14. Zhou JX, Liang YT, Liu ZX et al. On-chip integrated waveguide amplifiers on erbium-doped thin-film lithium niobate on insulator. *Laser Photonics Rev* **15**, 2100030 (2021).
15. Liang YT, Zhou JX, Liu ZX et al. A high-gain cladded waveguide amplifier on erbium doped thin-film lithium niobate fabricated using photolithography assisted chemo-mechanical etching. *Nanophotonics* **11**, 1033–1040 (2022).
16. Cai ML, Wu K, Xiang JM et al. Erbium-doped lithium niobate thin film waveguide amplifier with 16 dB internal net gain. *IEEE J Sel Top Quantum Electron* **28**, 8200608 (2022).
17. Yan CL, Wang SQ, Zhao S et al. A short high-gain waveguide amplifier based on low concentration erbium-doped thin-film lithium niobate on insulator. *Appl Phys Lett* **122**, 123503 (2023).
18. Wu JW, Yan XS, Wang XY et al. Efficient integrated amplifier-assisted laser on erbium-doped lithium niobate. *ACS Photonics* **11**, 2114–2122 (2024).
19. Cai ML, Li TY, Zhang XJ et al. Gain dynamics in integrated waveguide amplifier based on erbium-doped thin-film lithium niobate. *ACS Photonics* **11**, 4923–4932 (2024).
20. Wu RB, Wang M, Xu J et al. Long low-loss-litium niobate on insulator waveguides with sub-nanometer surface roughness. *Nanomaterials* **8**, 910 (2018).
21. Wang M, Wu RB, Lin JT et al. Chemo-mechanical polish lithography: a pathway to low loss large-scale photonic integration on lithium niobate on insulator. *Quantum Eng* **1**, e9 (2019).
22. Bao R, Fang ZW, Liu J et al. An erbium-doped waveguide amplifier on thin film lithium niobate with an output power exceeding 100 mW. *Laser Photonics Rev* **19**, 2400765 (2025).
23. Wu RB, Gao L, Liang YT et al. High-production-rate fabrication of low-loss lithium niobate electro-optic modulators using photolithography assisted chemo-mechanical etching (PLACE). *Micromachine* **13**, 378 (2022).
24. Zhang MR, Wu JY, Zhao ZY et al. Efficient and polarization insensitive edge coupler based on cascaded vertical waveguide tapers. *Opt Express* **31**, 31796–31805 (2023).
25. Huang CH, McCaughan L, Gill DM. Evaluation of absorption and emission cross sections of Er-doped $LiNbO_3$ for application to integrated optic amplifiers. *J Lightwave Technol* **12**, 803–809 (1994).
26. Thiel CW, Macfarlane RM, Böttger T et al. Optical decoherence and persistent spectral hole burning in Er^{3+}: $LiNbO_3$. *J Lumin* **130**, 1603–1609 (2010).
27. Brinkmann R, Baumann I, Dinand M et al. Erbium-doped single- and double-pass Ti: $LiNbO_3$ waveguide amplifiers. *IEEE J Quantum Electron* **30**, 2356–2360 (1994).
28. Huang CH, McCaughan L. 980-nm-pumped Er-doped $LiNbO_3$ waveguide amplifiers: a comparison with 1484-nm pumping. *IEEE J Sel Top Quantum Electron* **2**, 367–372 (1996).
29. Veasey DL, Gary JM, Amin J et al. Time-dependent modeling of erbium-doped waveguide lasers in lithium niobate pumped at 980 and 1480 nm. *IEEE J Quantum Electron* **33**, 1647–1662 (1997).

30. Dinard M, Sohler W. Theoretical modeling of optical amplification in Er-doped Ti: $LiNbO_3$ waveguides. *IEEE J Quantum Electron* **30**, 1267–1276 (1994).
31. Giles CR, Desurvire E. Modeling erbium-doped fiber amplifiers. *J Lightwave Technol* **9**, 271–283 (1991).
32. Desurvire E, Zyskind JL, Simpson JR. Spectral gain hole-burning at 1.53 μm in erbium-doped fiber amplifiers. *IEEE Photonics Technol Lett* **2**, 246–248 (1990).
33. Han JL, Li MQ, Dong QN et al. Suppression of parasitic lasing in erbium doped thin film lithium niobate waveguide amplifier by integrated wavelength division multiplexer. *APL Photonics* **9**, 126108 (2024).

Acknowledgements

We are grateful for financial supports from National Key R&D Program of China (Grant No. 2022YFA1205100, 2022YFA1404600), National Natural Science Foundation of China (Grant Nos. 12192251, 12334014, 12474325, 12134001, 12304418, 12474378, 12274133, 12174107, 12174113, 12274130), the Innovation Program for Quantum Science and Technology (Grant No. 2021ZD0301403), Shanghai Municipal Science and Technology Major Project (Grant No. 2019SHZDZX01), Fundamental Research Funds for the Central Universities, the Engineering Research Center for Nanophotonics & Advanced Instrument, Ministry of Education, East China Normal University (No. 2023nmc005).

Author contributions

All authors have accepted responsibility for the entire content of this manuscript and approved its submission.

Competing interests

The authors declare no competing financial interests.

Supplementary information

Supplementary information for this paper is available at https://doi.org/10.29026/oes.2025.250004